

# Synbeads Porous-Rigid Methacrylic Support: Application to Solid Phase Peptide Synthesis and Characterization of the Polymeric Matrix by FTIR Microspectroscopy and High Resolution Magic Angle Spinning NMR

Loris Sinigoi,<sup>†</sup> Paola Bravin,<sup>†</sup> Cynthia Ebert,<sup>†</sup> Nicola D'Amelio,<sup>‡,§</sup> Lisa Vaccari,<sup>||</sup> Laura Ciccarelli,<sup>⊥</sup> Sara Cantone,<sup>#</sup> Alessandra Basso,<sup>\*,†,#</sup> and Lucia Gardossi<sup>†</sup>

Laboratory of Applied and Computational Biocatalysis, Dipartimento di Scienze Farmaceutiche, Università degli Studi di Trieste, Piazzale Europa, 1-34127 Trieste, Italy, Bracco Imaging S.p.A., CRB Trieste, AREA Science Park, Q building, S.S. 14, Km 163.5, I-34012, Basovizza, Trieste, Italy, CBM Srl—Consorzio per il Centro di Biomedicina Molecolare, AREA Science Park, S.S. 14, km 163, 5 Basovizza, 34149 Trieste, Italy, Elettra Synchrotron Light Laboratory, SISSI, AREA Science Park, S.S. 14, Km 163.5, 34012 Basovizza, Trieste, Italy, Resindion S.r.l., Mitsubishi Chemical Corporation, Via Roma 55, 20082, Binasco (MI), Italy, and SPRIN s.r.l., c/o Università degli Studi di Trieste, Piazzale Europa, 1-34127 Trieste, Italy

Received March 30, 2009

Porous and rigid methacrylic Synbeads were optimized and applied efficiently to the solid phase peptide synthesis with the objective of improving significantly volumetric yields (0.33 mol/L calculated on the basis of maximum chemical accessibility, i.e. the maximum number of functional groups that can be acylated by FmocCl) as compared to swelling commercial polymers (from 0.06 to 0.12 mol/L). The effects of the density of functional groups and spacer length were investigated obtaining a chemical accessibility of the functional groups up to 1 mmol/g<sub>dry</sub>. High resolution magic angle spinning (HR-MAS) was exploited to evidence the presence of “solution-like” flexible linkers anchored on the rigid methacrylic backbone of Synbeads and to study the degree of functionalization by the Wang linker. To demonstrate the efficiency of the optimized Synbeads, the peptides Somatostatin and Terlipressin were synthesized. In the case of Somatostatin, final synthetic yields of 45 and 60% were achieved by following the HCTU/DIPEA and DIC/HOBt routes respectively, with the HPLC purity always higher than 83%. In the case of Terlipressin, the synthesis was carried out in parallel on Synbeads and also on TentaGel, ChemMatrix, and PS-DVB for comparison (DIC/HOBt route). The profiles describing the synthetic efficiency demonstrated that Synbeads leads to synthetic efficiency (86%) comparable to PS-DVB (96%) or ChemMatrix (84%). In order to gain a more precise picture of chemical and morphological features of Synbeads, their matrix was also characterized by exploiting innovative approaches based on FTIR microspectroscopy with a conventional source and with synchrotron radiation. A uniform distribution of the functional groups was evidenced through a detailed chemical mapping.

## Introduction

Research in solid phase peptide synthesis (SPPS) has shown rapid growth since this synthetic strategy moves toward automation and miniaturization for the production of a wide array of compounds. On the other hand, large scale solid phase synthesis (SPS) is gaining industrial interest, due to the increasing demands of peptidic drugs.<sup>1–6</sup>

A number of different materials have proven to be useful supports for SPPS and for solid-phase enzymatic peptide

synthesis (SPEPS),<sup>7</sup> such as polystyrene,<sup>8</sup> poly(ethylene glycol)–polystyrene graft polymers (i.e., TentaGel),<sup>9</sup> poly(ethylene glycol),<sup>10</sup> polyacrylamides,<sup>11</sup> PEGA polymers and their derivatives,<sup>12–18</sup> ChemMatrix,<sup>19</sup> silica and its derivatives,<sup>20</sup> and many other miscellaneous supports.<sup>7</sup> However, not all of them are compatible with the different types of solvents and reagents, so the proper support must be selected for each specific application. The general requirements of the support to be used in automated and large scale SPPS are mechanical stability, chemical inertness, consistency of loading, and bead size. Moreover, good diffusion of reagents in the support is requested, which is generally achieved by using insoluble matrixes endowed with swelling capacity. Nonswelling supports, such as silica and derivatives, find marginal applications in SPPS due to their small particle size and low loading capacity caused by their low porosity and

\* To whom correspondence should be addressed. Fax: (+3904052572). Tel.: (+390405583110). E-mail: basso@sprinttechnologies.com.

<sup>†</sup> Università degli Studi di Trieste.

<sup>‡</sup> Bracco Imaging S.p.A.

<sup>§</sup> CBM Srl - Consorzio per il Centro di Biomedicina Molecolare.

<sup>||</sup> Elettra Synchrotron Light Laboratory.

<sup>⊥</sup> Resindion s.r.l.

<sup>#</sup> SPRIN s.r.l.

**Table 1.** Effect of the Density of Amino Groups on the Chemical Accessibility

entry	name	theoretical loading <sup>a</sup> (mmol/g <sub>dry</sub> )	TEC <sup>b</sup>	PV <sup>c</sup> (mL/g)	SSA <sup>d</sup> (m <sup>2</sup> /g)	CA <sup>e</sup>	
						(mmol/g <sub>dry</sub> )	(%)
1	Synbeads <sup>21</sup>	2.50	1.58			0.06	4
2	Synbeads A310	1.00	0.94	1.41	29	0.88	94
3	Synbeads A308	0.85	0.86	1.31	35	0.78	91
4	Synbeads A306	0.60	0.57	1.30	21	0.46	81
5	Synbeads A304	0.40	0.40	1.38	21	0.36	90
6	Synbeads A302	0.30	0.35	1.15	43	0.29	83
7	Synbeads A300	0.15	0.17	1.07	46	0.16	94

<sup>a</sup> Functional groups theoretically present on the polymers (based on mass balance). <sup>b</sup> Total exchange capacity (primary amino group density). <sup>c</sup> Pore volume: mercury injection method with Autopore 9220. <sup>d</sup> Specific surface area: BET single-point method with Flowsorb 2300. <sup>e</sup> Chemical accessibility (determined by Fmoc number), i.e. the maximum number of functional groups that can be acylated.<sup>21</sup>

consequent limited accessibility.<sup>20</sup> Nevertheless, the use of rigid nonswelling supports would allow the reduction of the reaction volumes and solvent consumption, as long as the loading and chemical accessibility are assured through optimal and tunable porosity.

Recently, we have reported the use of Synbeads, a new class of nonswelling polymers, in the chemo-enzymatic synthesis of peptides.<sup>21</sup> Synbeads are rigid and macroporous methacrylic supports that combine mechanical stability with reproducible bead size and chemical distribution of the functional groups. The porosity (pore diameter >2000 Å) can be tuned in order to ensure diffusion of reactants, even as large as enzymes.<sup>21</sup> Results obtained with the first generation of Synbeads confirmed their applicability in chemical and biocatalysed processes and demonstrated that the development of rigid and highly porous polymers is a route to be pursued.<sup>21</sup>

In the present work we report on the optimization of Synbeads in terms of chemical accessibility and loading with the ultimate objective of improving synthetic efficiency and volumetric yields. The applicability of Synbeads in solid phase peptide synthesis was demonstrated by synthesizing Somatostatin and Terlipressin and by comparing also the results obtainable with other commercial polymers. Finally, the new optimized Synbeads were characterized by making use of a spectroscopic approach based on FTIR microspectroscopy ( $\mu$ -FTIR). Among the analytical methods that have been developed for monitoring of combinatorial reactions on solid phase,<sup>22–27</sup> FTIR  $\mu$ -spectroscopy on a single resin bead allows to detect the appearance or disappearance of functional groups carried by building blocks or protecting groups during chemical reactions.<sup>28–31</sup>

## Results and Discussion

### Chemical and Structural Optimization of Synbeads.

The first aim of this study was to improve the chemical accessibility of the functional groups on the Synbeads.

Polymers presenting the spacer 6-aminohexyl were used for the study that was focused on the evaluation of the influence of functional groups density. The concentration of the monomer bearing the functional group was reduced during the polymerization: the theoretical loading was reduced from 2.5 mmol/g<sub>dry</sub> (Table 1, entry 1, corresponding to the original Synbeads previously described)<sup>21</sup> to values ranging from 0.15 to 1 mmol/g<sub>dry</sub>, following a standard suspension polymerization method.<sup>32</sup> As a result, six new samples of Synbeads were produced, which differ in porosity and functional groups density. All Synbeads included in the set listed in Table 1 are 6-aminohexyl-fuction-

alized, and the chemical accessibility, i.e. the maximum number of functional groups that can be acylated, was evaluated by means of the Fmoc method (see experimental). Table 1 illustrates how, by maintaining the group density (expressed as theoretical loading) below 1 mmol/g<sub>dry</sub>, the chemical accessibility increases from 4 to above 80% (entries 2–7, Table 1).

It is interesting to note that in the case of new developed Synbeads (entries 2–7) presenting low functional group density, the total exchange capacity is in good agreement with the theoretical concentration of amino groups and this indicates optimal distribution of functional groups in the matrix and their complete accessibility.

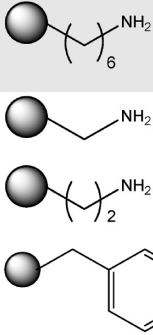
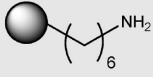
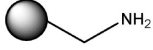

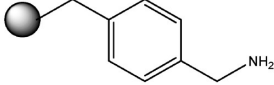
It must be underlined that the optimization of the density of functional groups allowed the chemical accessibility of Synbeads to increase from 4% (entry 1<sup>21</sup>) up to 94% (entry 7, 0.15 mmol/g<sub>dry</sub>).

The effect of spacers different from 6-aminohexyl were evaluated. The ratio of the monomers was maintained equal to the case of A310, whereas different terminal amino spacers were used. Table 2 shows the characterization of these polymers prepared using aliphatic and aromatic spacers as aminomethyl, 2-aminoethyl, 6-aminohexyl, and 4-aminomethylbenzyl. Results indicate that, as expected, a long linear spacer such as 6-aminohexyl improves the reactivity, i.e. chemical accessibility, whereas an aromatic and rigid linker has the opposite effect (Table 2). Therefore, among the different samples of Synbeads that were prepared, Synbeads A310, functionalized with a long and linear spacer, 6-aminohexyl (entry 1, Table 2), represent the best compromise in terms of functional group density (1 mmol/g<sub>dry</sub>), chemical accessibility (94%), and linker structure.

Table 3 compares the theoretical maximum mmoles of peptide achievable per volumetric unit of reactor (i.e., volumetric yield) obtainable with Synbeads A310 and A302 and with different commercial polymers. Thanks to the low solvent retention, Synbeads A310 allow the theoretical volumetric yield to increase from 2- to 5-fold as compared to PS-DVB, which is the commercial polymer endowed with the lowest solvent retention among those tested.<sup>33,34</sup> The advantage is even more evident when TentaGel and Chem-Matrix are considered.

**Analysis through High Resolution Magic Angle Spinning NMR.** HR-MAS was exploited to study the degree of functionalization of Synbeads. This technique allows the analysis of inhomogeneous or semisolid samples, by exploiting magic angle spinning (MAS) to average out the main causes of NMR line broadening (namely chemical shift

**Table 2.** Effect of the Spacer on Chemical Accessibility of Synbeads

Terminal group		TEC <sup>a</sup>	Chemical accessibility <sup>b</sup>	
		mmol/g <sub>dry</sub>	mmol/g <sub>dry</sub>	%
Synbeads A310		0.94	0.88	94
Synbeads functionalised with aminomethyl-		0.97	0.27	28
Synbeads functionalised with 2-aminoethyl-		0.55	0.40	73
Synbeads functionalised with 4-aminomethylbenzyl-		0.97	0.46	47

<sup>a</sup> Total exchange capacity (primary amino group density). <sup>b</sup> Chemical accessibility (determined by Fmoc number).

**Table 3.** Theoretical Volumetric Yields Obtained with Different Polymers

polymer	loading (mmol/g <sub>dry</sub> )	dry volume (mL/g <sub>dry</sub> )	swelling volume (mL/g)					maximum volumetric yield <sup>a</sup> (mmol/mL of reactor volume)
			water	DMF	MeOH	NMP	DCM	
Synbeads A310	1.0	2.5	3.0 <sup>b</sup>	3.0 <sup>b</sup>	3.0 <sup>b</sup>	3.0 <sup>b</sup>	3.0 <sup>b</sup>	0.33
Synbeads A302	0.3	2.5	3.0 <sup>b</sup>	3.0 <sup>b</sup>	3.0 <sup>b</sup>	3.0 <sup>b</sup>	3.0 <sup>b</sup>	0.10
TentaGel	0.3 <sup>c</sup>	1.7	3.6	4.7	3.6	4.6	6.3	0.06
PS-DVB	0.7 <sup>c</sup>	1.6		5.6	2.0	5.7	8.3	0.12
ChemMatrix	0.7 <sup>c</sup>	n.d.	11	8.5	9.0	8.5	12	0.08

<sup>a</sup> Maximum millimoles of peptide achievable per volumetric unit of reactor, calculated considering the minimum amount of DMF necessary to condition the resin and guarantee reagents diffusion. <sup>b</sup> Variation in volume due to the external shell of solvation. <sup>c</sup> Declared by the supplier.

anisotropy and dipolar interaction). HR-MAS has proven useful for characterization of polymers,<sup>35–38</sup> for monitoring reaction sequences, for determining enantiomeric excess directly on supports, for resin quantification, and for monitoring peptide synthesis.<sup>39</sup> In our experiments, we exploited the ability of HR-MAS to monitor only nuclei able to interact with a solvent, thus distinguishing solution-like flexible parts (functional groups) from the rigid backbone of Synbeads.

<sup>1</sup>H HR-MAS NMR spectra of the Synbeads presented in this work confirmed both the rigidity of the matrix and the flexibility of the linked functional groups. The <sup>1</sup>H HR-MAS spectrum of Synbeads A310 coupled with a Wang linker is shown in Figure 1A. As expected, no peak arising from the matrix is visible while the protons of the functional group are clearly recognizable in the aromatics signals around 7 ppm. These signals are not due to exchangeable protons as <sup>1</sup>H,<sup>13</sup>C heteronuclear single quantum coherence (HSQC) experiments demonstrated that they are attached to aromatic carbons (data not shown). Furthermore they cannot belong to the matrix as it does not contain aromatic moieties. Finally, they cannot derive from unbound functionalizing molecules as their line width is significantly larger than that of a fast tumbling species.

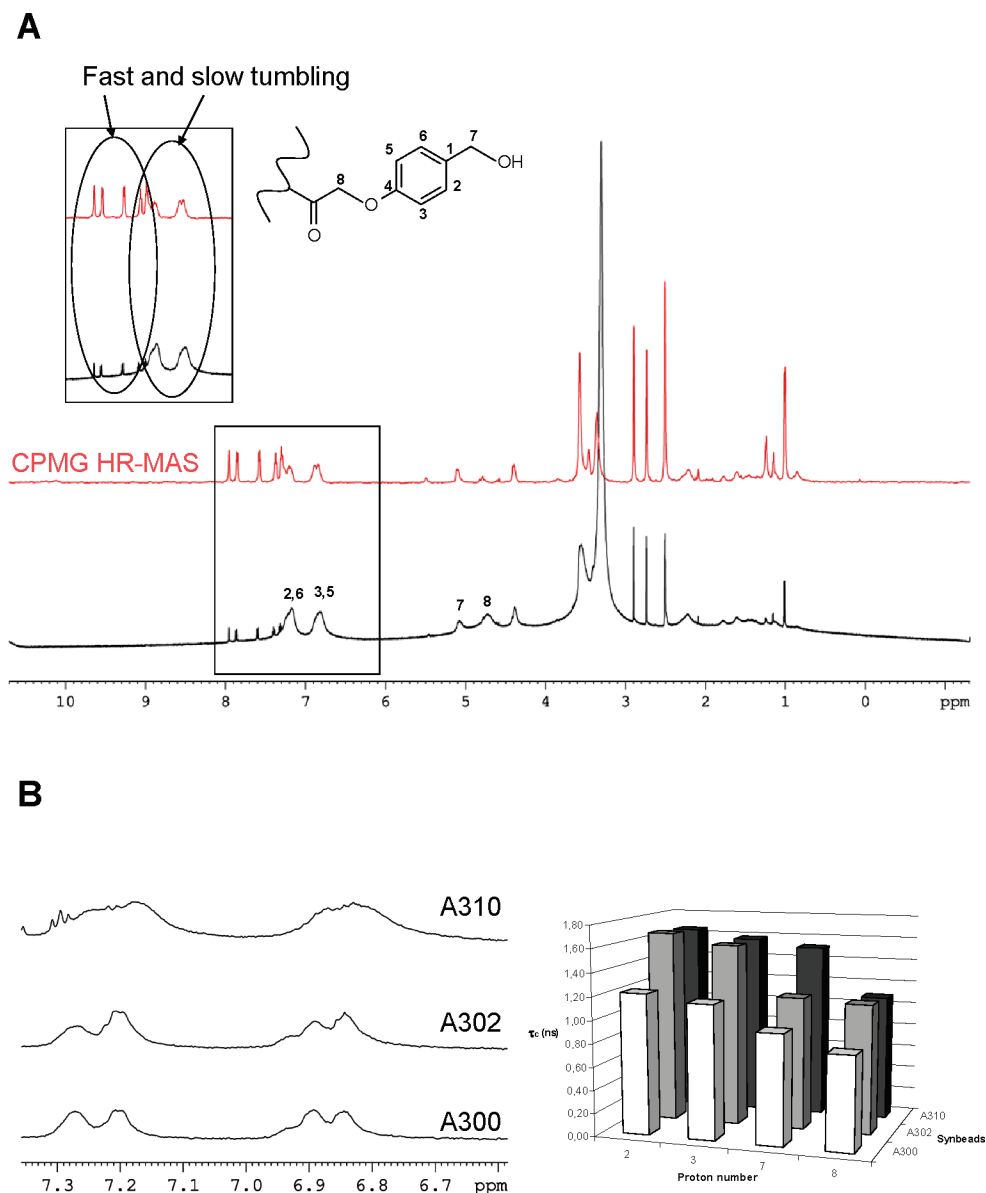
Proton and carbon assignment was obtained by heteronuclear multiple bond correlation spectroscopy (HMBC) and nuclear Overhauser effect spectroscopy (NOESY) experiments and is shown in Table 4. Experiments have been proposed to separate signals of the polymer from residual solvents exploiting the different diffusion coefficient.<sup>40</sup> Diffusion ordered spectroscopy (DOSY) experiment demonstrated that all the assigned signals belong to the polymer (data not shown). A Carr–Purcell–Meiboom–Gill (CPMG)

filter (displayed in red in the Figure 1A) can be applied to better discriminate between fast and slow tumbling molecules as it tends to suppress the latter. As expected, in the CPMG spectrum small molecules (residual solvents and reagents) are enhanced with respect to the slowly tumbling ones.

The mobility of the functionalizing groups is important for their reactivity and solvent accessibility. Interestingly, as suggested by the differences in line width among different polymers, the mobility of the Wang linker decreases when the degree of derivation is higher (Synbeads A310 in Figure 1B), most likely because of steric hindrance among the linker moieties. This effect is further demonstrated by the decreased mobility of Synbeads A310, as compared to Synbeads A302 or Synbeads A300 where the signals show the largest line width. In order to demonstrate this effect we measured both longitudinal ( $R_1$ ) and transversal ( $R_2$ ) relaxation rates (Table 4). As expected for relaxation modulated by dipolar mechanism in large molecules ( $\omega_H\tau_c \gg 1$  with  $\omega_H$  being the nuclear frequency of hydrogen and  $\tau_c$ , the correlation time),  $R_1$  decreases and  $R_2$  increases going from A300 to A310 indicating a slowing of motion (longer  $\tau_c$ ).

The correlation time can be estimated by the ratio  $R_1/R_2$  which is independent of the unknown internuclear distance of the protons causing relaxation (eq 1):<sup>41</sup>

$$\frac{R_1}{R_2} = \frac{\frac{6\tau_c}{(1 + \omega_H^2\tau_c^2)} + \frac{24\tau_c}{(1 + 4\omega_H^2\tau_c^2)}}{\frac{15\tau_c}{(1 + \omega_H^2\tau_c^2)} + \frac{6\tau_c}{(1 + 4\omega_H^2\tau_c^2)} + 9\tau_c} \quad (1)$$



**Figure 1.** (A) Conventional  $^1\text{H}$  and  $^1\text{H}$  CPMG (red) HR-MAS spectra of Wang Synbead A310; HR-MAS NMR spectra show profiles similar to the solution state. The signals from the rigid methacrylic backbone of the matrix remain beyond detection. (B, left)  $^1\text{H}$  HR-MAS spectra of Synbeads A300, A302, and A310 functionalized with a Wang linker, showing the effect of the increased functionalization (see Table 4). (B, right) Correlation times ( $\tau_c$ , ns) derived from relaxation data demonstrating a slowing of the motion (larger values) as a function of the degree of derivatization.

**Table 4.** NMR Assignment and Proton Relation Rates in A300, A302, and A310

atom number <sup>c</sup>	$^1\text{H}$ (ppm)	$^{13}\text{C}$ (ppm)	$R_1$ ( $\text{s}^{-1}$ ) <sup>a</sup>			$R_2$ ( $\text{s}^{-1}$ ) <sup>b</sup>		
			A300	A302	A310	A300	A302	A310
2	7.25	130.2	0.61	0.60	0.59	11.4	19.8	18.9
3	6.88	115.0	0.63	0.62	0.60	10.3	17.8	17.9
7	5.09	66.1	1.09	1.04	0.73	12.9	17.2	20.2
8	4.72	64.9	1.08	0.85	0.80	9.7	13.5	12.1

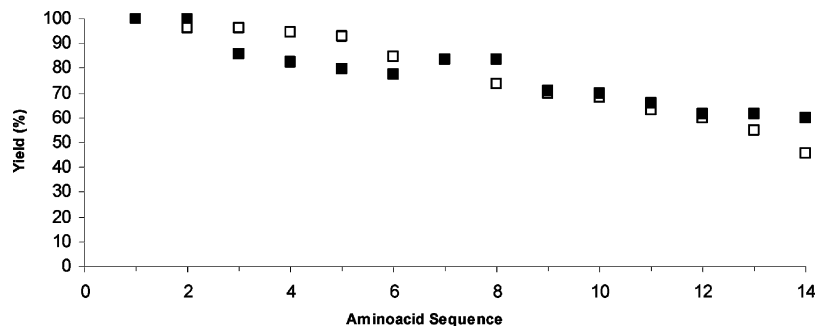
<sup>a</sup> Longitudinal relaxation rate. <sup>b</sup> Transversal relaxation rate. <sup>c</sup> For atom number, see Figure 1A.

The values calculated in this way (Figure 1B) have limited precision (as a detailed mathematical description of the motion is not considered in the equation), but they indicate clearly that the motion slows down going from A300 to A310.

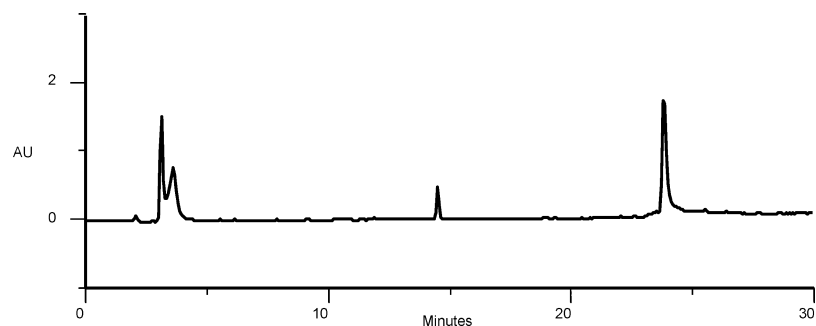
Differences in mobility make it difficult to correctly estimate the degree of chemical modification by the intensity of the signals of samples, even when prepared in identical

conditions. This is due to differential signal loss caused by transversal relaxation.

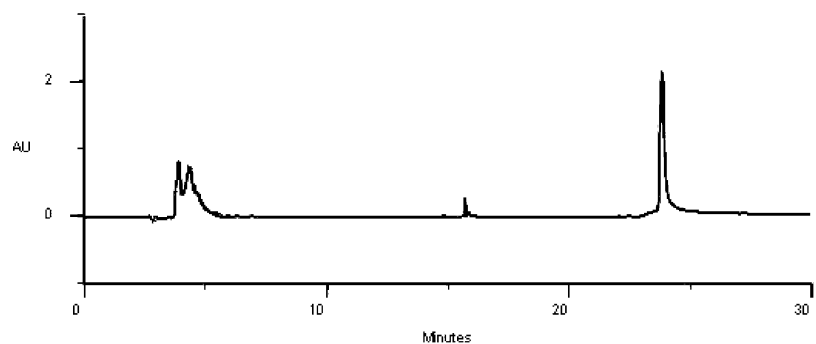
**Application of Synbeads to the Synthesis of Somatostatin and Terlipressin.** Two batches of the new optimized Synbeads, namely Synbeads A310 and Synbeads A302 (Table 1), were applied in the solid phase synthesis of two pharmaceutically relevant peptides to demonstrate their practical applicability.



**Figure 2.** Synthetic yield of Somatostatin using the DIC/HOBt (black squares) and HCTU/DIPEA (empty squares) strategies.



**Figure 3.** HPLC profile of Somatostatin from Synbeads using the HCTU/DIPEA method (RT = 24 min,  $\lambda = 220$  nm, purity 84%). After synthesis, the peptide was cleaved by TFA and the solution was analyzed by RP-HPLC (see the Experimental Section).



**Figure 4.** HPLC profile of Somatostatin from Synbeads using the DIC/HOBt method (RT = 24 min,  $\lambda = 220$  nm, purity 91%). After synthesis the peptide was cleaved by TFA and the solution was analyzed by RP-HPLC (see the Experimental Section).

Synbeads A310 was used for the synthesis of a Somatostatin, a 14 aminoacids hormone, with a disulfide bridge between Cys1 and Cys12. The synthesis was performed following the Fmoc/tBu approach and using the Rink amide linker which was coupled on the polymer by the DIC/HOBt route obtaining a loading of 0.31 mmol/g<sub>dry</sub> (determined by Fmoc number).

The hormone was synthesized following two different strategies: DIC/HOBt and HCTU/DIPEA. HCTU is a new and advanced activator that has found large application due to the presence of the chlorine that makes this reagent highly reactive.<sup>42</sup> Carbodiimides (as DIC) are highly effective due to the formation of a reactive species (*O*-acylisourea) and are used especially in large scale synthesis because of their moderate cost (HCTU is roughly ten times more expensive than DIC).

The efficiency of two synthetic routes was compared, and results are summarized in Figure 2.

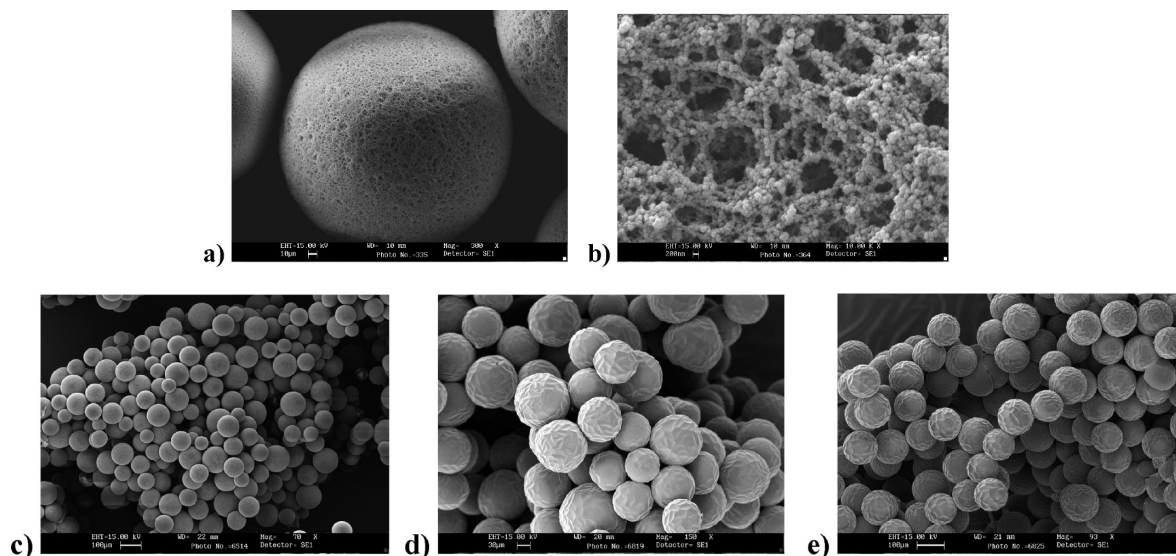
The DIC/HOBt route gives profiles similar to the HCTU/DIPEA approach (Figure 2), with a higher final yield (60% compared to 45%), which makes the classical DIC/HOBt strategy preferable, also in terms of costs of reagents.

The HPLC profiles in Figures 3 and 4 indicate the purity of the crude Somatostatin as recovered from the Synbeads A310. The crude product, obtained by cleavage with TFA and ether precipitation, was characterized also by ES-MS showing the presence of the target peptide at  $m/z = 1639.8$ .

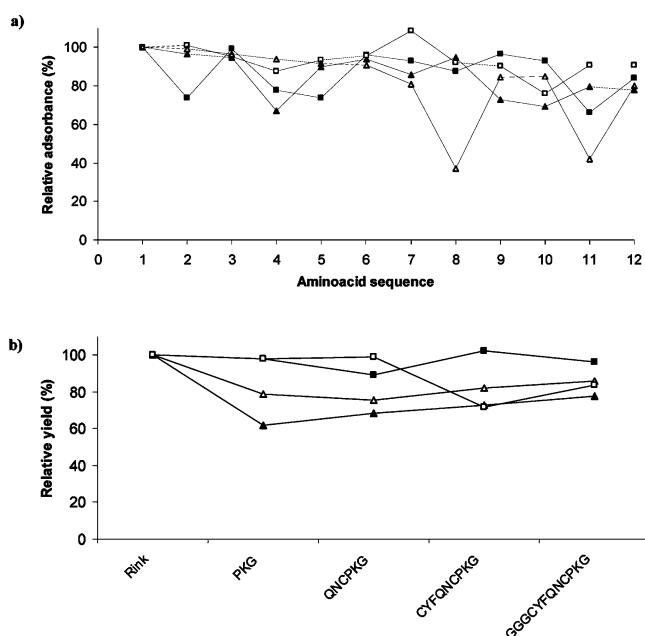
In the case of Terlipressin, the synthesis was carried out in parallel on Synbeads A302 but also on TentaGel, ChemMatrix, and PS-DVB for comparison. Terlipressin is a synthetic analog of the natural hormone Vasopressin, formed by 12 aminoacids and a terminal chain of Gly, and it has found large application in therapy in the acute esophageal variceal hemorrhage and septic shock.

In this case, Synbeads A302, which have a theoretical loading of 0.3–0.4 mmol/g<sub>dry</sub>, were used in order to have a direct comparison with TentaGel that has a loading of 0.3 mmol/g as well. Two other commercial resins, namely PS-DVB and ChemMatrix, were also used, which present higher initial loading (around 0.7 mmol/g<sub>dry</sub>, Table 3).

Figure 5 shows the differences between a rigid polymer such as Synbeads A310 and swelling polymers: Synbeads are characterized by a macroporosity that assures good



**Figure 5.** SEM microscopy of Synbeads A310 (a and b); PS-DVB (c); ChemMatrix (d); and TentaGel (e).

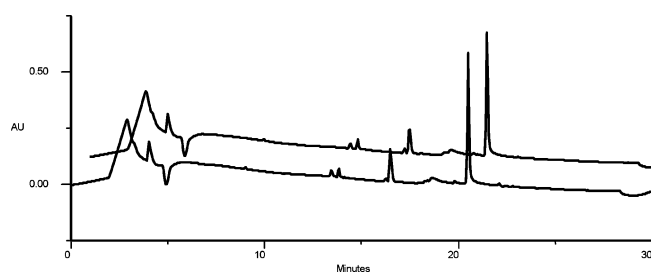


**Figure 6.** (a) Relative adsorbance (290 nm) determined by Fmoc removal after each coupling step. (b) Relative ponderal yields, determined considering the mass increase of the polymer during the synthesis of Terlipressin, after the synthesis of the first three aminoacids (PKG), six aminoacids (QNCPKG), nine aminoacids (CYFQNCPKG), and twelve aminoacids (GGGCYFQNCPKG) on PS-DVB (black squares), Synbeads A302 (empty triangle), ChemMatrix (empty squares), and TentaGel (black triangles).

diffusion, whereas swelling polymers in their dry state are characterized by their typical roughness.

The synthesis of Terlipressin was performed by the DIC/HOBt strategy using the Rink amide linker, and the adsorbance was monitored after each coupling step (Figure 6a).

As shown in Figure 6b, the relative ponderal yields on PS-DVB, Synbeads A302, ChemMatrix and TentaGel were 96, 86, 84, and 78%, respectively. The relative ponderal yield is an important indicator of the efficiency of the synthetic strategy, and it clearly shows how Synbeads and PS-DVB lead to the highest relative yields. This result indicates that in the case of Terlipressin the swelling capacity is not the key factor for an efficient peptide synthesis.



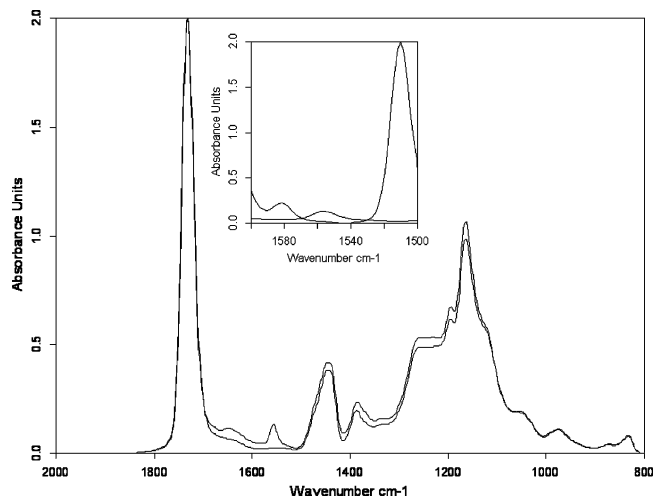
**Figure 7.** (a) HPLC profile of crude Terlipressin from Synbeads. (b) HPLC profile of crude Terlipressin from PS-DVB.

In all cases, Terlipressin was analyzed by ES-MS (showing a signal at 1229.6  $m/z$ ) and HPLC (Figure 7) after synthesis, cleavage with TFA, and ether precipitation.

The superimposed HPLC profiles shown in Figure 7 indicate that the peptide can be obtained with comparable purity on both polymers.

#### Analysis of Functional Group Distribution and Study of Diffusion Phenomena in Synbeads by Means of FTIR Microspectroscopy

When optimizing supports for solid phase synthesis, it is very important to ensure that the reagents also enter the core of the rigid beads and react promptly even with the buried functional groups. However, microscopic techniques usually applied to access these data, such as those based on staining or radio- or fluorescence labeling, can introduce artifacts or cannot be directly applied to nonoptically transparent Synbeads. For example, two-photon microscopy, widely applied on optically transparent polymers,<sup>43</sup> cannot be applied to rigid and opaque Synbeads; therefore, an imaging approach for bead accessibility studies, based on  $\mu$ -FTIR, was adapted and optimized for Synbeads.<sup>44–46</sup> Infrared spectroscopy is a label-free, quantitative, and nondestructive technique for chemical characterization of a material through the detection of its characteristic vibrational modes. This chemical information can be spatially resolved exploiting capabilities of vis-IR microscopes ( $\mu$ -FTIR), both using single-point and bidimensional focal plane array (FPA) IR detectors (see the Experimental Section for more details).



**Figure 8.** ATR-FTIR spectra of unfunctionalized (gray) and 60 min functionalized (black) beads are compared upon normalization to carbonyl ester band. A nitro group stretching band centered at  $1555\text{ cm}^{-1}$  can be clearly recognized. In the inset, the epoxy embedding resin FTIR spectrum (light gray) is compared in the region of interest with the functionalized bead spectrum.

Specifically,  $\mu$ -FTIR and conventional attenuated total reflection (ATR) FTIR spectroscopy have been exploited to monitor a test reaction: amidation of amino-terminated A310 Synbeads with 3-nitropropionic acid. The amidation was performed in DMF (see the Experimental Section), and a ninhydrin test<sup>47</sup> indicated reaction completion within 1 h. For experimental purposes, samples of the polymer were withdrawn at different reaction times (10, 20, 30, 40, and 60 min) and immediately rinsed with DMF in order to stop the reaction and to eliminate reagents adsorbed but not covalently bound to the matrix (as verified by HPLC analysis). For  $\mu$ -FTIR experiments, both crude and nitropropionic acid functionalized Synbeads A310 were cut in  $5\text{-}\mu\text{m}$  thin slices after their inclusion in a commercial epoxy-based resin. Since the resin diffuses inside Synbeads' pores, the embedding resin was carefully chosen among the available ones in order not only to ensure a good resistance to cut forces but also to avoid the overlapping of its characteristic IR-bands with those of Synbeads (see inset of Figure 8). Figure 8 shows the ATR-FTIR (see the Experimental Section) spectra of the not-embedded Synbeads A310 and of the same matrix after 60 min of functionalization through amidation reaction. The FTIR spectrum of the methacrylic matrix is dominated by the carbonyl stretching of ester bond centered at  $1736\text{ cm}^{-1}$ . The clearer difference between unfunctionalized and functionalized matrix is the band centered at  $1555\text{ cm}^{-1}$ , only present in the functionalized samples and characteristic for the asymmetric stretching vibration of the  $\text{NO}_2$  group. In the inset of Figure 8, the spectrum of 60 min functionalized A310 bead is compared in the  $1600\text{--}1500\text{ cm}^{-1}$  region with the spectrum of epoxy embedding resin. Two specific embedding resin bands at  $1508$  and  $1584\text{ cm}^{-1}$  can be seen, but they are separated enough from the nitro band to avoid any band deconvolution during data analysis.

FTIR-ATR spectra on ground beads of Synbeads A310 at intermediated functionalization times were also collected (data not shown) demonstrating that in the first 10 min the

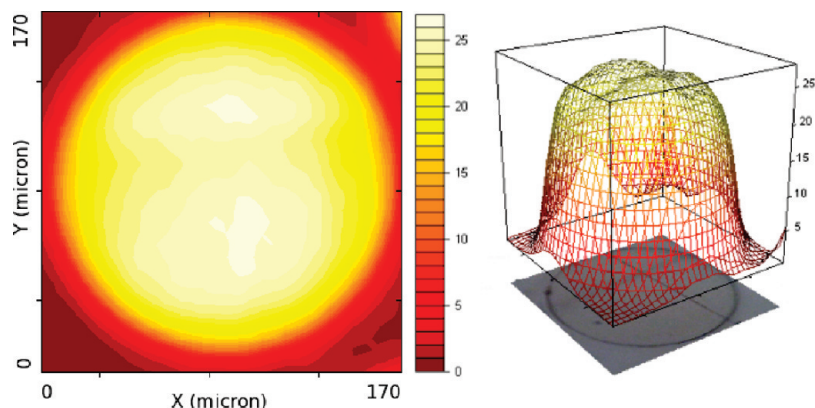
reaction progressed to the 70%, reaching about 90% in 30 min, to be completed in 60 min. The degree of advancement of the chemical reaction was estimated calculating the nitro/ester band area ratio and normalizing at 60 reaction minutes (reaction completed). These data have been confirmed by  $\mu$ -FTIR, as detailed in the following.

Chemical images of the beads at different reaction times have been acquired in transmission mode ( $15\times$  condenser and objective) using a bidimensional FPA detector operated with conventional Globar source. In this configuration, the imaged region has an area of about  $170 \times 170\ \mu\text{m}^2$  (pixel resolution  $\sim 2.6\ \mu\text{m}$ ). In order to fit equatorial bead's sections in the detector field of view, Synbeads have been selected in size of  $150\text{--}200\ \mu\text{m}$  through filtration on controlled porosity filters before functionalization.

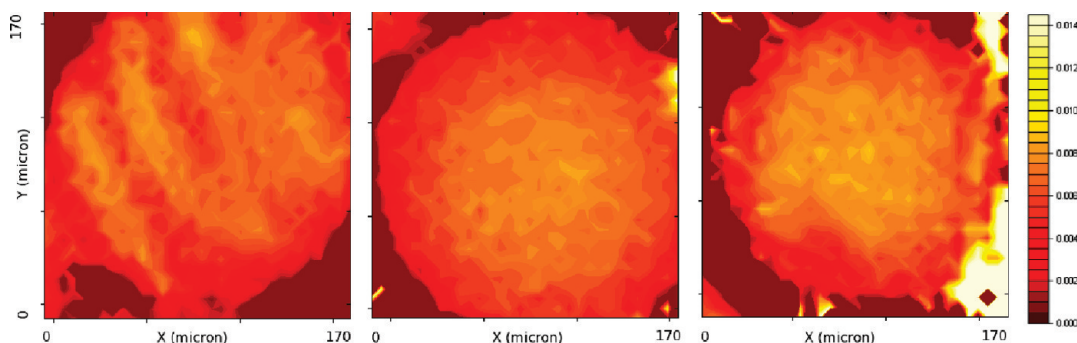
Figure 10 shows the distribution of carbonyl ester group in unfunctionalized Synbeads A310 obtained by applying the univariate functional group mapping approach: the carbonyl ester band was integrated (integration frequency limits:  $1764\text{--}1681\text{ cm}^{-1}$ ), and integral values were plotted both using a 2D (Figure 9a) and 3D (Figure 9b) representation. The imaged bead, which has a diameter of about  $170\ \mu\text{m}$ , is characterized by an external shell of about  $30\ \mu\text{m}$  where the carbonyl ester group integral fast increases from 0 to 24 au while in the inner part it maintains values ranging from 24 to 26 au. This distribution can be considered quite homogeneous at the bead core level, without the presence of clusters and aggregations, and reflects the homogeneous polymerization mechanism of Synbeads.

Slices corresponding to functionalized samples at different reaction times (10, 40, and 60 min) were also imaged. In order to reduce image artifacts due to thickness inhomogeneity and/or cut defects, in Figure 10 the ratio between the nitro-band integral ( $1567\text{--}1544\text{ cm}^{-1}$ ) and the carbonyl band integral ( $1764\text{--}1681\text{ cm}^{-1}$ ) is plotted. Referring to Figure 11, it is possible to assert that the degree of functionalization of the beads does not change significantly in time, confirming FTIR-ATR experiments, and that the bead external shell is less functionalized than the bead core, that is then accessible in the first reaction minutes. It is possible to notice that, within the first reaction minutes, some bead regions seem to be preferentially functionalized (yellower stripes in Figure 10 left); this "clusterlike" distribution of nitro functional groups, however, disappears while the reaction proceeds, turning in a "domelike" one, already present at 40 reaction minutes (Figure 10 center), due to a progressive accumulation of product reaction mainly at the bead core level.

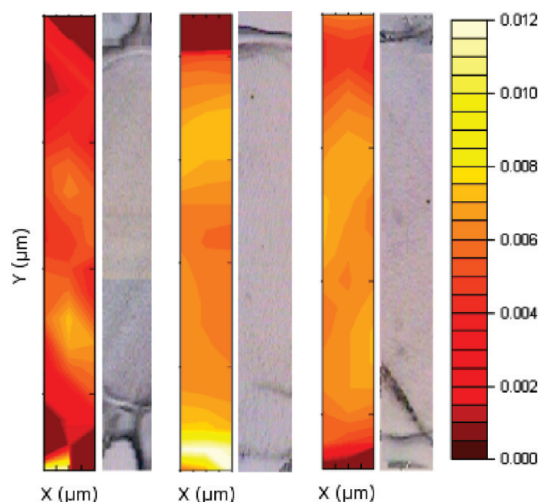
$\mu$ -FTIR is a fast and noninvasive chemical imaging method; however, when the concentration of the species of interest is very low, such as the one of the nitro-functional group,  $\mu$ -FTIR data of better spectral quality can be achieved exploiting the high brightness of the synchrotron radiation (SR) source. Diagonal bead sections  $30\ \mu\text{m}$  wide were mapped at a  $10\ \mu\text{m}$  spatial resolution, shining more light on the Synbeads accessibility by reagents (see Figure 11). SR  $\mu$ -FTIR confirmed the lower degree of functionalization of the bead shell when compared with the bead core at each reaction time; however, the relative concentration of the nitro



**Figure 9.** 2D (a) and 3D (b) chemical images of the carbonyl group distribution (integration interval 1764–1681  $\text{cm}^{-1}$ ). The color scale represents the integral values in arbitrary units (au). The optical image of the bead section is also shown at the bottom of the 3D sketch. Data has been collected with 64 accumulation scans and 4  $\text{cm}^{-1}$  spectral resolution (conventional source, bidimensional FPA detector). Atmospheric compensation and  $2 \times 2$  pixel binning routines of the OPUS program have been run before integration. The spatial resolution is about 5.3  $\mu\text{m}$ .



**Figure 10.** Nitro group distribution normalized on the carbonyl group after 10, 40, and 60 min of reaction. Data has been collected with 64 accumulation scans and 4  $\text{cm}^{-1}$  spectral resolution (conventional source, bidimensional FPA detector). Atmospheric compensation and  $2 \times 2$  pixel binning routines of the OPUS program have been run before integration.



**Figure 11.** Nitro group distribution normalized on the carbonyl group after 10, 40, and 60 min of reaction. Data has been collected with 512 accumulation scans, 4  $\text{cm}^{-1}$  spectral resolution, and 10  $\mu\text{m}$  spatial resolution (SR source, MCT detector). Optical images of mapped sections are also reported. Sections are 190, 200, and 180  $\mu\text{m}$  long, respectively. Atmospheric compensation has been run before integration.

group at the bead center is slightly lower than the surroundings, revealing a small but detectable bead accessibility decrease.

From these studies, it is possible to conclude that Synbeads present a homogeneous polymeric matrix and that reagents

can rapidly reach the core of the beads, leading to an almost homogeneous and complete functionalization of the polymer, even if SR  $\mu$ -FTIR mapping highlighted a lower degree of functionalization at the bead center. However, in order to obtain the better spectra quality of SR data we need to take into account the much longer acquisition time and the nondirect accessibility of SR facilities. A combination of SR  $\mu$ -FTIR imaging, with a conventional source and FPA detector, and SR infrared microspectroscopy, along with conventional spectroscopic tools, has to be considered the best approach to access qualitative and quantitative information on diffusion phenomena inside a nontransparent support matrix for SPS in general and SPPS in particular.

## Conclusions

The expansion of the applications of solid phase organic synthesis calls for new classes of solid supports. Scalability, easy handling, and tunable micro and macro properties are major priorities for the development of the new generation of solid matrices which are expected to match emerging technological requests going from large scale production of peptides at lower costs to facilitation of downstream processing of fine chemicals. This work describes how a novel class of rigid polymers, Synbeads, has been developed and optimized by combining chemical and chemical–physical studies. The nonswelling properties of the methacrylic matrix has been translated into a major technological advantage only



after tailoring the polymer porosity and by studying in detail the chemical functionalization of the support. The practical applicability of Synbeads has been demonstrated not only experimentally but also through the detailed analysis of accessibility and diffusion of substrates by exploiting  $\mu$ -FTIR and HR-MAS NMR.

The results indicate that Synbeads represent an efficient new class of solid supports that can be further tailored and exploited for matching new technological and synthetic challenges in the field of solid phase chemistry.

## Experimental Section

**Materials.** Standard Synbeads and functionalized Synbeads were from SPRIN s.r.l. Free samples for research use are available upon request.<sup>48</sup> All chemicals were obtained from Sigma-Aldrich or IRIS Biotech and were used without further purification. All the solvents, prior to use, were dried over molecular sieves (4Å). *N,N*-Dimethylformamide (DMF) used in acylation reactions was Biotech grade, >99% (Aldrich).

PS-DVB (aminomethyl polystyrene resin cross-linked 1% DVB, loading 0.7 mmol/g), TentaGel S NH<sub>2</sub> (loading of amino groups 0.29 mmol/g), and ChemMatrix (aminomethyl-ChemMatrix resin, loading 0.66 mmol/g) were from Iris Biotech.

Reactions were conducted using a solvent (DMF)/polymer ratio of 10–11 mL/g.

**Solvent Retention.** The solvent retained polymers amount was quantified on the basis of the weight difference between wet and dried resins (heated overnight at 110 °C).

**Ninhydrin Test.** Three solutions were prepared: solution A with 5 g ninhydrin in 100 mL ethanol; solution B with 80 g phenol in 20 mL ethanol; solution C with 2 mL of a KCN solution (0.01 M in water) added to 98 mL pyridine. One drop of each solution was added on small amount (less than 10 mg) of resin. The mixture was then heated to 200 °C. A blue color was evidence of the presence of nonreacted primary amines, while a yellow color indicated all amines had reacted.

**Fmoc Number Determination.** The Fmoc number was determined according to procedures reported in the literature.<sup>49</sup>

**Preparation of Preloaded Polymers (with HMPA or Rink Amide Linker).** A solution of linker (HMPA or Rink amide linker) (3 equiv), DIC (4 equiv), and HOBt (6 equiv) in DMF was added to polymers. The reaction was maintained for 3 h at room temperature under constant stirring on a blood rotator (40 rpm). At the end of the reaction, the resin was filtered and washed with MeOH, DCM, and DMF. HMPA linker was used in the HR MAS study.

**Synthesis of Somatostatin.** The Somatostatin was synthesized on Synbeads A310 derivatized with Rink linker using both the DIC/HOBt/DMAP<sup>50–53</sup> and HCTU/DIPEA protocols.<sup>54,55</sup>

**DIC/HOBt/DMAP Protocol.** A solution of *N*<sup>α</sup>-Fmoc-AA (4 equiv), DIC (5 equiv), HOBt (7 equiv), and DMAP (0.1 equiv) in DMF/NMP 1:1 with Triton X and ethyl carbonate was added to Rink–Synbeads (0.31 mmol/g). Two coupling steps were done for each amino acid, and each coupling was

performed at 50 °C for 1 h in blood rotator. At the end of each coupling the resin was filtered and washed with MeOH, DCM, and DMF. Once the resin was found negative to Kaiser test, a solution of acetic anhydride (10 equiv) in DMF was added to the resin and the reaction was performed at room temperature for 1 h. After the capping procedure, the *N*<sup>α</sup>-Fmoc protecting group was removed and assessed using a UV spectrophotometer at  $\lambda = 290$  nm. All the amino acids were incorporated using the same protocol.

**HCTU/DIPEA Protocol.** A solution of *N*<sup>α</sup>-Fmoc-AA (5 equiv), HCTU (4.9 equiv), and DIPEA (10 equiv) in DMF/NMP 1:1 with Triton X and ethyl carbonate was added to Rink–Synbeads (0.31 mmol/g). The reaction was maintained at 50 °C for 1 h in blood rotator. Two coupling steps were done for each amino acid. At the end of the incorporation of each amino acid, the resin was filtered and washed with MeOH, DCM, and DMF. Once the resin was found negative to ninhydrin test, a solution of acetic anhydride (10 equiv) in DMF was added to the resin and the reaction was performed at room temperature for 1 h. After the capping procedure, the *N*<sup>α</sup>-Fmoc protecting group was removed and assessed using UV spectrophotometer at  $\lambda = 290$  nm. All the amino acid were incorporated using the same protocol. The peptide was characterized by HPLC and ES-MS.

**Synthesis of Terlipressin.** Swelling resins (PS, TentaGel, and ChemMatrix), previously functionalized with Rink linker, were preswelled in 5 mL/g of DMF for 10 min, then a solution of *N*<sup>α</sup>-Fmoc-AA (3 equiv), DIC (4 equiv), and HOBt (6 equiv), dissolved in 5 mL (per gram of resin) of DMF, was added. Differently, in the case of Synbeads, no pre-swelling is required and a solution of *N*<sup>α</sup>-Fmoc-AA (3 equiv), DIC (4 equiv), and HOBt (6 equiv), dissolved in 10 mL/g of DMF, was directly added to the Rink functionalized Synbeads.

The reaction was performed twice for each amino acid coupling, at room temperature for 30 min. At the end of the incorporation of each amino acid, the resins were filtered and washed with MeOH, DCM, and DMF. Once the resins were found negative to ninhydrin test, a solution of acetic anhydride (10 equiv) in DMF was added to the polymers, and the reaction was performed at room temperature for 1 h. After the capping procedure, the *N*<sup>α</sup>-Fmoc protecting group was removed and assessed using UV spectrophotometer at  $\lambda = 290$  nm. All coupling were performed using the same protocol. The peptide was characterized by HPLC and ES-MS.

**Cleavage and Characterization.** The peptides were cleaved using a solution of TFA 95% for 1 h at room temperature in a blood rotator. Then, the resin was filtered and ice-cold diethyl ether was added to TFA solution in order to precipitate the protein. Once ether was evaporated, the peptide was characterized with C-18 RP-HPLC and ES-MS.

**HPLC Analysis.** Analyses were performed using a Gilson HPLC system (321 pump, 232XL autoinjector and 170 DAD UV system) equipped with a C<sub>18</sub> Chrompack column. The conditions were as follows: flow 1 mL/min, gradient from 90/10 water/acetonitrile to 10/90 water/acetonitrile in 35 min. Both phases containing 0.01% TFA. Products were analyzed

at 220–260 nm. Purity were calculated by peaks integration (220 nm spectrum, TFA peak integration excluded).

**ES-MS Analyses.** APII (Perkin-Elmer SCIEX) electron-spray ionization was used. Spectra were collected by generating positively charged ions that plunge in a gap of mass/charge ratios of 400 and 2400 *uma*. The conditions were as follows: flow 10  $\mu\text{L}/\text{min}$  (acetonitrile in water 49.5%, formic acid 1%), capillary voltage 4500–5000 V.

**Reaction of Synbeads with 3-Nitropropionic Acid.** A known amount of Synbeads A310 was transferred in a reaction syringe and washed with MeOH/DMF (50:50 v/v), MeOH, DCM, and DMF. 3-nitropropionic acid (3 equiv) and DIC (3 equiv) in DMF were added. The mixture was maintained at 25 °C under stirring (blood rotator). Samples of the reaction mixture were taken at 5, 10, 20, 30, and 60 min reaction times and immediately washed to stop the reaction. On each sample, a ninhydrin test was conducted.

Blanks were made reacting Synbeads A310 with 3-nitropropionic acid (3 equiv) in DMF. The mixture was maintained at 25 °C under stirring (blood rotator). Samples of the reaction mixture were taken at 5, 10, 20, 30, and 60 min reaction times and were immediately washed. On each sample, a ninhydrin test was conducted. Ground blanched Synbeads were analyzed by means of the ATR  $\mu\text{-FTIR}$  technique to confirm that no nitropropionic acid was adsorbed on Synbeads.

**NMR.** Samples for HR-MAS were prepared using 8 mg of Synbeads and 60  $\mu\text{L}$  of deuterated DMSO. HR-MAS experiments were performed on a 600 MHz spectrometer Bruker Avance III Ultra Shield Plus operating at 600.17 MHz, available at CBM, Trieste. A Bruker HR-MAS 4 mm rotor probe head, equipped with a deuterium lock channel and double coils designed for  $^{13}\text{C}$ – $^1\text{H}$  inverse detection was employed. Spectra were acquired with a spinning rate of 4000 Hz. For CPMG experiments, an echo half-time of 0.5 ms was used; the echo was recycled 60 times. NMR assignment was achieved by NOESY (mixing time of 50 ms to avoid spin diffusion),  $^1\text{H}$ ,  $^{13}\text{C}$ -HSQC, and  $^1\text{H}$ ,  $^{13}\text{C}$ -HMBC (using a delay optimized for a  $J = 6$  Hz).  $R_1$  and  $R_2$  relaxation rates were measured by inversion recovery and CPMG pulse sequences without solvent suppression. DOSY with bipolar gradients was performed using big and little deltas of 400 and 4.4 ms, respectively.

**FTIR Spectroscopy and Microspectroscopy.** FTIR measurements have been performed at the infrared beamline SISSI at Sincrotrone Elettra Trieste.

Synbeads A310 were sieved by means of a 65 mesh sieve to obtain a uniform sample of beads with a particle size of 160–200  $\mu\text{m}$ . Sieved Synbeads A310 were functionalized with 3-nitropropionic acid (3 equiv) and DIC (3 equiv) in DMF at 25 °C and dried with DCM. Part of the sample was then ground in a mortar, and single-reflection ATR spectra with conventional source were acquired (single-reflection ATR accessory MIRacle, PIKE technologies, Vertex 70 Interferometer, Bruker, mercury–cadmium–telluride detector, 512 accumulation scans, 4  $\text{cm}^{-1}$ , background on a clean Ge hemisphere) in order to monitor the advancement of the reaction.

Beads of each sample were also included in an epoxy resin and cut in 5- $\mu\text{m}$  slices using an ultra microtome. Slice integrity and dragging of the inclusion resin onto the beads were verified at CSPA (Trieste) by means of transmission electron microscopy (Philips EM 208) and scanning electron microscopy (SEM Leica Stereoscan 430i). Bead slices with a diameter of 160–200  $\mu\text{m}$ , corresponding to the equatorial part of the beads, were imaged with a conventional source using a bidimensional FPA detector (Hyperion 3000 Vis/IR microscope, Bruker, Vertex 70 interferometer, Bruker, 64 accumulation scans, 4  $\text{cm}^{-1}$  spectral resolution). The employed FPA is a 64  $\times$  64 pixel detector with a 2.5  $\times$  2.5  $\text{mm}^2$  detector area. It allows simultaneously acquiring 4096 spectra with a pixel resolution dependent on the employed IR objective. Synchrotron radiation infrared maps were acquired at 10  $\mu\text{m}$  spatial resolution, 4  $\text{cm}^{-1}$  spectral resolution, coadding 512 scans per map point (Hyperion 3000 Vis/IR microscope, Bruker, Vertex 70 interferometer, Bruker).

**Acknowledgment.** A.B. thanks Università degli Studi di Trieste for financial support. We thank Bruker Biospin srl for providing the HR-MAS NMR apparatus, CBM (Consorzio per il Centro di Biomedicina Molecolare S.c.r.l., AREA Science Park, Basovizza, Trieste, Italy) for hosting the instrumentation, and Bracco Imaging Spa for providing the technical staff. The authors thank Dr. Thomas Bruckdorfer for stimulating and fruitful discussion.

## References and Notes

- (1) *Peptide synthesis protocols*; Pennington, M. W., Dunn, B. M., Eds.; Humana Press: Totowa, 1994; Vol. 35, p 91.
- (2) *Synthetic peptides*; Grant, G., Ed.; W. H. Freeman and Co.: New York, 1992.
- (3) Fields, G. B.; Noble, R. L. *Int. J. Peptide Protein Res.* **1990**, *35*, 161–214.
- (4) *Chemical approaches to the synthesis of peptides and proteins*; Lloyd-Williams, P., Albericio, F., Eds.; CRC Press: New York, 1997.
- (5) Chan, W. C.; White, P. D. *Fmoc solid phase peptide synthesis: a practical approach*; Oxford University Press: Oxford, 2000.
- (6) Bruckdorfer, T.; Marder, O.; Albericio, F. *Curr. Pharm. Biotechnol.* **2004**, *5*, 29–43.
- (7) Basso, A.; Braiuca, P.; Ebert, C.; Gardossi, L.; Linda, P. *J. Chem. Technol. Biotechnol.* **2006**, *81*, 1626–1640.
- (8) Merrifield, R. B. *J. Am. Chem. Soc.* **1963**, *85*, 2149–2154.
- (9) Bayer, E. *Angew. Chem., Int. Ed. Engl.* **1991**, *30*, 113–117.
- (10) Harris, J. M. *J. Macromol. Sci. C., Rev. Macromol. Chem. Phys.* **1985**, *C25*, 325–373.
- (11) Arshady, R.; Atherton, E.; Clive, D. L. J.; Sheppard, R. C. *J. Chem. Soc., Perkin Trans. 1* **1981**, 529–537.
- (12) Meldal, M. *Tetrahedron Lett.* **1992**, *33*, 3077–3080.
- (13) Meldal, M.; Auzanneau, F.-I.; Hindsgaul, O.; Palcic, M. M. *J. Chem. Soc. Chem. Commun.* **1994**, 1849–1850.
- (14) Renil, M.; Meldal, M. *Tetrahedron Lett.* **1996**, *34*, 6185–6188.
- (15) Tornøe, C. W.; Meldal, M. *Tetrahedron Lett.* **2002**, *43*, 6409–6411.
- (16) Groth, T.; Grötli, M.; Lubell, V. D.; Miranda, L. P.; Meldal, M. *J. Chem. Soc., Perkin Trans.* **2000**, 4258–4264.
- (17) Rademann, J.; Grötli, M.; Meldal, M.; Bock, K. *J. Am. Chem. Soc.* **1999**, *121*, 5459–5466.
- (18) Miranda, L.; Lubell, W.; Halkes, K.; Groth, T.; Grötli, M.; Rademann, J.; Gottfredsen, C.; Meldal, M. *J. Comb. Chem.* **2002**, *4*, 523–539.
- (19) Garcia Martin, F.; Quintanar Audelo, M.; Garcia Ramos, Y.; Cruz, J. L.; Gravel, C.; Furic, R.; Coté, S.; Tulla Puche, J.; Albericio, F. *J. Comb. Chem.* **2006**, *8*, 213–220.

- (20) Basso, A.; De Martin, L.; Ebert, C.; Linda, P.; Gardossi, L.; Ulijn, R. V.; Flitsch, S. L. *Tetrahedron Lett.* **2003**, *44*, 6083–6085.
- (21) Basso, A.; Braiuca, P.; De Martin, L.; Ebert, C.; Gardossi, L.; Linda, P.; Verdelli, S.; Tam, A. *Chem.—Eur. J.* **2004**, *10*, 1007–1013.
- (22) Yan, B. *Acc. Chem. Res.* **1998**, *31*, 621–630.
- (23) Egner, B. J.; Bradley, M. *DDT* **1997**, *2*, 102–109.
- (24) Meldal, M. *Biopolym. (Peptide Sci.)* **2002**, *6*, 93–100.
- (25) Kress, J.; Zanaletti, R.; Amour, A.; Ledlow, M.; Frey, J. G.; Bradley, M. *Chem.—Eur. J.* **2002**, *8*, 3769–3772.
- (26) Kress, J.; Rose, A.; Frey, J. G.; Brocklesby, W. S.; Ladlow, M.; Mellor, G. W.; Bradley, M. *Chem.—Eur. J.* **2001**, *7*, 3880–3883.
- (27) Rademann, J.; Barth, M.; Brock, R.; Egelhaaf, H.-J.; Jung, G. *Chem.—Eur. J.* **2001**, *7*, 3884–3889.
- (28) Yan, B.; Kumaravel, G.; Anjaria, H.; Wu, A.; Petter, R., Jr.; Jewell, C. F.; Wareing, J. R. *J. Org. Chem.* **1995**, *60*, 5736–5738.
- (29) Yan, B.; Kumaravel, G. *Tetrahedron* **1996**, *52*, 843–848.
- (30) Haap, W. J.; Walk, T. B.; Jung, G. *Angew. Chem., Int. Ed.* **1998**, *37*, 3311–3314.
- (31) Li, W.; Yan, B. *J. Org. Chem.* **1998**, *63*, 4092–4097.
- (32) *Prodotti di supporto per la sintesi in fase solida e processo per la loro preparazione.* Patent no. MI2007A000782, April 2007.
- (33) Bouillon, I.; Soural, M.; Müller, M. J.; Krchová, V. *J. Comb. Chem.* **2009**, *11*, 213–215.
- (34) García-Martín, F.; Quintanar-Audelo, M.; García-Ramos, Y.; Cruz, L. J.; Gravel, C.; Furic, R.; Côté, S.; Tulla-Puche, J.; Albericio, F. *J. Comb. Chem.* **2006**, *8*, 213–220.
- (35) Guinó, M.; de Miguel, R. Y. In *Analysis and Purification Methods in Combinatorial Chemistry*; Yan, B., Ed.; John Wiley & Sons, Inc.: New York, 2004; Vol. 163, Chapter 4, pp 71–86.
- (36) Shapiro, M. J.; Gounarides, J. S. *Prog. Nucl. Magn. Reson. Spectrosc.* **1999**, *35*, 153–200.
- (37) Fruchart, J. S.; Lippens, G.; Kuhn, C.; Gras-Masse, H.; Melnyk, O. *J. Org. Chem.* **2002**, *67*, 526–532.
- (38) Schröder, H. *Comb. Chem. High Throughput Screen.* **2003**, *6*, 741–753.
- (39) Shapiro, M. J.; Gounarides, J. S. *Biotechnol. Bioeng.* **2000–2001**, *71*, 130–148, and references therein.
- (40) Chin, J.; Shapiro, M. J. *Magn. Reson. Chem.* **2000**, *38*, 782–784.
- (41) Freeman, R.; Hill, H. D. W.; Tomlinson, B. L.; Hall, L. D. *J. Chem. Phys.* **1974**, *61*, 4466–4473.
- (42) *The Bachem Practice of SPPS*; Mergler, M., Durieux, J. P., Eds.; Bachem AG: Switzerland, 2000.
- (43) Deere, J.; McConnel, G.; Lalaoui, A.; Maltman, B. A.; Flitsch, S. L.; Halling, P. J. *Adv. Synth. Catal.* **2007**, *349*, 1321–1326.
- (44) Yan, B.; Gremlich, H. G. *J. Chromatogr. B* **1999**, *725*, 91–102.
- (45) Haap, W. J.; Walk, T. B.; Jung, G. *Angew. Chem., Int. Ed.* **1998**, *37*, 3311–3314.
- (46) Mei, Y.; Miller, L.; Gao, W.; Gross, R. A. *Biomacromolecules* **2003**, *4*, 70–74.
- (47) Kaiser, E.; Colescott, R. L.; Bossinger, C. D.; Cook, P. I. *Anal. Biochem.* **1970**, *34*, 595–598.
- (48) SPRIN s.r.l., www.sprinttechnologies.com. Contact info for samples: Dr. Alessandra Basso, basso@sprinttechnologies.com.
- (49) Atherton, E.; Sheppard, R. C. In *Solid Phase Peptide Synthesis: A Practical Approach*; IRL Press: Oxford, 1989.
- (50) Wang, S. S.; Tam, J. P.; Wang, B. S. H.; Merrifield, R. B. *Int. J. Peptide Protein Res.* **1981**, *18*, 459–467.
- (51) Gamet, J.-P.; Jacquier, R.; Verducci, J. *Tetrahedron* **1984**, *40*, 1995–2001.
- (52) Takeda, K.; Ayabe, A.; Suzuki, M.; Konda, Y.; Harigaya, Y. *Synthesis* **1991**, *68*, 9–691.
- (53) Kuisle, O.; Quinoa, E.; Riguera, R. *J. Org. Chem.* **1999**, *64*, 8063–8075.
- (54) Marder, O.; Shvo, Y.; Albericio, F. *Chimica Oggi* **2002**, *7/8*, 37–41.
- (55) di Faenza, A.; Tancredi, M.; Galoppini, C.; Rovero, P. *Tetrahedron Lett.* **1998**, *39*, 8529–8532.

CC900050T